Scanning Microscopy

Volume 1 | Number 4 Article 14

7-29-1987

Analysis of Thick Targets by Proton-Induced X-Ray Emission

J. L. Campbell
University of Guelph

A. Perujo
University of Guelph

W. J. Teesdale
University of Guelph

J. A. Maxwell
University of Guelph

Scanning Microscopy, Vol. 1, No. 4, 1987 (Pages 1631-1640) 0891-7035/87$3.00+.00
Scanning Microscopy International, Chicago (AMF O'Hare), IL 60666 USA

ANALYSIS OF THICK TARGETS BY PROTON-INDUCED X-RAY EMISSION

J.L. CAMPBELL*, A. PERUJO, W.J. TEESDALE and J.A. MAXWELL

Guelph-Waterloo Program for Graduate Work in Physics,
University of Guelph, Guelph, Ontario
Canada N1G 2W1

(Received for publication March 02, 1987, and in revised form July 29, 1987)

Abstract

Most published PIXE (proton-induced X-ray emission) work concerns thin targets. Recently progress in improving both the fundamental data base and in developing a range of standardization techniques has propelled thick target analysis to the forefront of activity in the PIXE field. Limits of detection are a complex issue depending not only on the continuous background but also on the characteristic X-rays of the matrix; in favorable cases a few ppm may be reached in convenient analysis times. The unfolding of multi-element PIXE spectra is akin to the same problem in EPMA (electron probe microanalysis), and EPMA methodologies, especially as regards background removal, have a role to play; accurate analytic lineshapes for Si(Li) detectors are a crucial ingredient of accurate extraction of peak areas. Analyses of a binary compound and of the NBS aluminum alloy SRM 1258 illustrate the current capabilities of TTPIXE (thick-target PIXE). Recent computer simulation work extends TTPIXE's capability from the customary smooth specimens to targets with curved or randomly rough surfaces.

KEY WORDS: Proton-induced X-ray emission, thick targets, data base, standardization, spectrum fitting.

*Address for correspondence:
J.L. Campbell
Guelph-Waterloo Program for Graduate Work in Physics, University of Guelph, Guelph, Ontario, Canada N1G 2W1. Phone No. (519)824-4120 x3124

Introduction

The early developmental stage of PIXE (proton-induced X-ray emission) analysis focussed mainly on thin targets. As the technique matured, experimental and computational methods for handling thick targets (i.e., thick enough to stop the typical 2-4 MeV proton beams) emerged, and now the variant called TTPIXE (thick target PIXE) is seeing routine use, especially in the context of microbeam analysis. TTPIXE was reviewed quite recently (4) and the physics data-base fundamental to it was also examined in detail (6). This paper will build on these two references, stressing more recent developments, utilizing the obvious analogy between EPMA (electron probe micro-analysis) and micro-PIXE, and including some of our current results.

It should be stressed that comparisons of the respective merits of EPMA and PIXE are fraught with danger; they should be made only under very carefully defined conditions. But a few general remarks may be useful at the outset concerning the energy-dispersive version of each (PIXE is almost always done with energy dispersion whereas EPMA uses both energy and wavelength dispersion). Ionization cross-sections are similar for electrons of a few tens of keV and protons of a few MeV energy, but the proton background continuum is much less intense. The resulting more favourable peak-to-background ratio for protons often offers the possibility of lower detection limits in a given specimen, typically 10-100 ppm in TTPIXE compared with 100-1000 ppm in EPMA. This puts more of a premium on highly efficient target-detector geometry in TTPIXE than in EPMA. In the early days of PIXE, the target chambers used were redolent of nuclear physics experiments; now TTPIXE proponents are drawing upon the integrated EPMA experience and are designing much more sophisticated specimen chambers, which often include detectors for gamma rays, backscattered ions and secondary electrons together with high-magnification light optics.

Formalism and Data-base for TTPIXE

For a thick, homogeneous target with

protons of energy E_o incident in the geometry of figure 1, the yield of Kα (or Lα) X-rays from an element Z (atomic mass A_Z) of concentration C_Z is:

$$Y(Z) = \left(\frac{N_{av}\omega_z b_z^{\alpha}\varepsilon_z}{A_z}\right) NC_z \int_{E_o}^{o} \frac{\sigma_z(E)T_z(E)dE}{S(E)} \quad , \qquad (1)$$

where $T_Z(E)$ is the photon attenuation

$$T_z(E) = \exp\left[-\left(\frac{\mu}{\rho}\right)\frac{\cos\alpha}{\sin\theta_{TO}}\int_{E_o}^{E}\frac{dE}{S(E)}\right] \quad . \qquad (2)$$

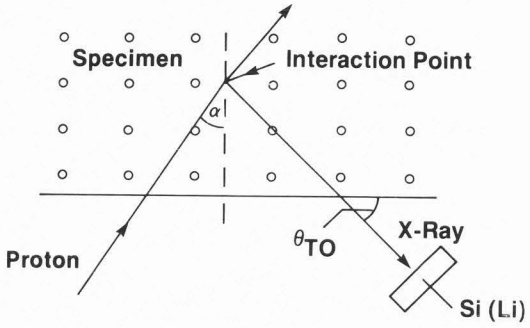

Fig. 1. Generalized geometry for TTPIXE analysis.

Here $\sigma_Z(E)$ is the ionization cross-section at energy E and S(E) the corresponding proton stopping power in the matrix; N is the number of incident protons and N_{av} Avogadro's number; ω_Z is the K (or L) X-ray fluorescence yield and b_Z^{α} the Kα (or Lα) fraction in the K (or L) X-ray series; ε_Z is the absolute detection efficiency including solid angle; μ/ρ is the mass attenuation coefficient for the Kα (or Lα) X-rays in the matrix. The integral is reminiscent of the ZAF correction in EPMA but is more easily calculated since the proton stopping is more easily modelled. An algorithm for economic computation of the integral is suggested in ref. (4). Secondary fluorescence requires addition of further terms to eq. (1).

Some of the quantities in equations (1) and (2) are shared by EPMA and TTPIXE but the proton stopping power and ionization cross-section are of course unique to the latter. Ref. (6) dealt with the manner in which errors in the data-base quantities were transmitted into errors in the X-ray yield. By proper choice of standardization technique (see below) the transmission of errors from the data base through the yield into final analyzed concentrations can be minimized.

Our previous view that the Andersen-Ziegler semi-empirical scheme (1) for stopping powers S(E) contributes negligibly to overall uncertainty is unchanged. But the situation as regards proton cross-sections is evolving steadily; this is demonstrated in two reviews (21,22) which assess the 1986 status of all available calculation schemes (theoretical and empirical) by comparing their results with 'reference' cross-sections; the latter are created by a sophisticated statistical analysis of all experimental data existing for all elements. Table 1 gives the reference values together with corresponding values from five schemes, in order to convey a flavour of the situation.

Most PIXE users have relied on the 1974 universal fit to data by Johansson and Johansson (17) which has the form:

$$\ell n(\sigma_K U_K^2) = \sum_{i=0}^{5} b_{K,i}[\ell n(E/\lambda U_K)]^i \qquad (3)$$

where U_K is the K-electron binding energy, λ = 1836.1514 and $b_{K,i}$ are the parameters given by Johansson and Johansson. While good at low Z, this falls low at high Z.

Currently the best combination of accuracy and convenience is afforded by Cohen and Harrigan's extensive tabulation (13) of cross-sections based on the ECPSSR theory (3) which employs perturbed stationary states and has corrections for energy loss (E), Coulomb effects (C) and relativity (R). New ECPSSR calculations (9) employing more sophisticated DHS* wave-functions are only a few percent different, but according to Paul (21) the discrepancy with theory is slightly reduced; these tables cover only $Z \geq 22$ and $0.1 < E < 3$ MeV. Our own software stores the parameters of fits of eq. (3) to ECPSSR-DHS cross-sections for each element independently, our attempts at more universal fits over a wide range of Z and E having been unsuccessful.

The deviation of the two ECPSSR treatments from experiment at low energies and large target Z values is due to the Coulomb correction used. Recent semi-classical (SCA) calculations (16) appear to be superior at low energies; they treat Coulomb deflection more accurately. However extensive results of these are not yet available to PIXE analysts. Various other schemes reviewed by Paul have more limited scope or are less accurate. The low-energy deviations of ECPSSR are not a serious drawback for TTPIXE since usually 2-4 MeV protons are employed and the bulk of the ionization occurs before their energy falls to 1 MeV.

The L-shell situation is rendered much more complex because measured L X-ray production cross-sections have to be converted to ionization cross-sections via fluorescence and Coster-Kronig yields. Most workers use Krause's compilation (19) for the latter, but there is a clear need for improvement in this data-base in view of the large uncertainties involved. The two ECPSSR tabulations referred to above cover the three L subshells, but the CH energy range (0.1-10 MeV) is more extensive than that of CC (0.1-3 MeV). In our own work the older 5-parameter Johansson and Johansson fit to σ_L has been superseded by fitting eq. (3) to the ECPSSR-DHS cross-sections for every element.

*Dirac-Hartree-Slater

Table 1.

K-shell ionization cross-sections (barns)

Target	E (MeV)	σ_{ref} (21,22)	σ by calculational schemes				
			Theoretical			Semi-Empirical	
			ECPSSR (13)	ECPSSR/DHS (9)	SCA (16)	JJ (17)	Khan (18)
Aℓ	0.5	6050± 600	6120			6247	4849
	1.0	17,400±1700	17,000			17,800	13,900
	2.0	29,300±2900	27,870			30,000	21,400
Cu	0.5	1.623±0.032	1.67	1.604		1.74	1.21
	1.0	15.90 ±0.32	16.52	15.63		15.88	14.5
	2.0	96.0 ±1.9	99.07	94.34		89.7	93.8
Ag	0.5	(3.77±0.3)(-3)	4.179 (-3)	4.043 (-3)	3.46 (-3)	1.63 (-3)	4.96 (-3)
	1.0	0.0829±0.0066	0.0827	0.0832	0.0841	0.055	0.087
	2.0	0.907 ±0.073	0.894	0.893	0.937	0.69	0.906

We turn now to quantities shared by TTPIXE and EPMA. The attenuation coefficient schemes favoured in EPMA are often based on fits of $(\mu/\rho) = CE^{-n}$ to experimental data (E is photon energy here). TTPIXE requires a rather wider photon energy range than most of the EPMA schemes and we therefore use the 1-40 keV scheme of Leroux and Thinh (20). Figure 2, taken from ref. (6), demonstrates how error in μ/ρ

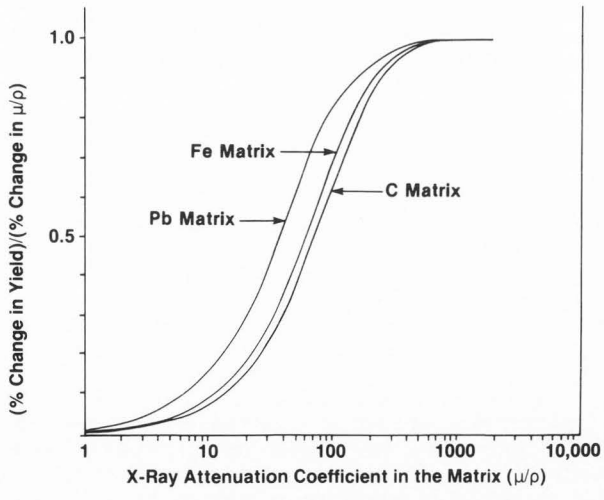

Fig. 2. Sensitivity of TTPIXE yields from 3 MeV protons to changes in matrix attenuation coefficient μ/ρ ($cm^2\ g^{-1}$) for K X-rays of most elements in C, Fe and Pb matrices.

transmits into X-ray yield; the quasi-universal behaviour is very useful. Ref. (6) judged that the yield uncertainty using the Leroux-Thinh scheme rose from ~1% at $\mu/\rho < 20\ cm^2\ g^{-1}$ to 5% at $\mu/\rho > 300\ cm^2\ g^{-1}$, with these numbers doubling near absorption edges. With TTPIXE in mind Gerward (15) has produced a new semi-empirical scheme for the 2-40 keV region. This includes further terms in the fits, for example to cater for scattering in addition to photo-electric absorption. It merits careful evaluation by TTPIXE users.

Fluorescence yields ω_K are known with accuracy $\lesssim$ 1% (2). The mean L-shell yield $\bar{\omega}_L$ for proton excitation has been calculated (11) using ECPSSR cross-sections (13) and Krause's subshell yield compilation (19); uncertainties vary across the periodic table and are strongly influenced by the 5-15% uncertainties of the compilation (19).

Accurate fractional intensities b_z for the various K X-ray lines are important not just for concentration determination via eq. (1) but for unfolding complex spectra with overlapping peaks. Most workers use the $K\beta/K\alpha$ ratios predicted by theory (27) or those from Salem et al.'s 1974 review (26) which suggests that for the third row elements $I(K\beta)/I(K\alpha)$ falls slightly below theory. Figure 3 adds post-review data to those of ref. (18). Despite sometimes large error bars the discrepancy is indeed clear for electron and photon excitation, but the scatter of proton data precludes any conclusions. We shall however shortly report

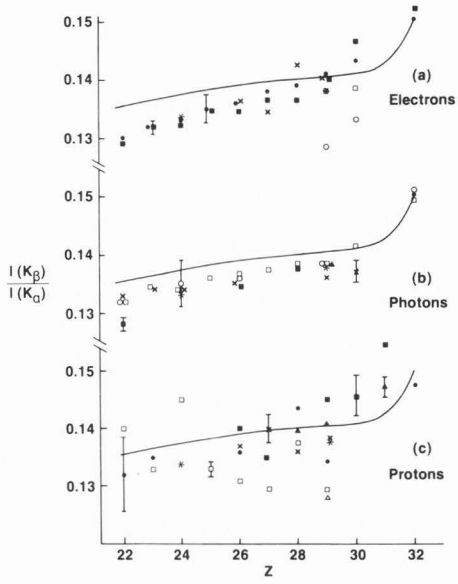

Fig. 3. Intensity ratios I(Kβ)/I(Kα) from a literature survey of experiments using electrons, photons and protons. The curve represents relativistic Hartree-Fock calculations (27).

new proton measurements which exhibit much the same trend as the upper two plots in figure 3. Relative L X-ray line intensities in PIXE depend not only on L subshell X-ray emission rates but also on the subshell cross-sections, fluorescence and Coster-Kronig yields. Cohen and Harrigan (12) present useful and extensive tables of intensities of 16 L lines for elements, calculated from a data-base of refs. (13), (19) and (26). Uncertainties in these are very hard to estimate, ranging typically from 5-15% but being sometimes much greater; clearly high accuracy experiments are needed to probe the data-bases (19) and (26).

Finally absolute Si(Li) detector efficiencies can be determined to 1-2% between 5 and 30 keV (5) by a combination of radionuclide standards and various diagnostic tests. From 1-4 keV, uncertainties could reach 10%.

Methods of Standardisation

Obviously eq. (1) and its associated data-base can be dispensed with if standards of the same matrix and trace elements are available. This happy situation is infrequent, especially in view of the difficulty of assuring homogeneity at the micron level.

Perhaps the other extreme is to adopt the thick single-element standards favoured frequently in EPMA. One then has:

$$C_Z = \frac{N_{ST}}{N_{SP}} \frac{Y_{SP}(Z)}{Y_{ST}(Z)} \cdot \frac{\int_{E_o}^{o} \frac{\sigma_Z(E) T_Z^{ST}(E) dE}{S_{ST}(E)}}{\int_{E_o}^{o} \frac{\sigma_Z(E) T_Z^{SP}(E) dE}{S_{SP}(E)}} \qquad (4)$$

where the suffixes ST and SP denote standard and specimen. An obvious advantage is the partial cancellation in eq. (4) of the cross-section and its energy-dependence, removing much of one of the major error sources. But the price paid is the introduction of a second photon attenuation factor (in the standard) and here there is no reason to expect error cancellation. The very different counting rates from standard and specimen are a further potential error source via pulse pile-up, beam charge measurement, etc.

Two examples of this approach are given in below, exemplifying the cases of known and unknown matrices.

Something of a compromise approach is to use a small number of synthetic standards of general similarity to the specimens as done by Remond et al. (24) at this conference. There a range of sulfide mineral matrices are analysed for trace elements from Ga to Cd via one synthetic iron sulfide containing traces of Se and Pd. Experimental/instrumental factors in eq. (1) are split off from the matrix factors by writing the X-ray yield for a defined proton charge as:

$$Y(Z,M) = H_Z C \quad I(Z,M) \; \varepsilon_Z^I \exp(-\mu x)_{abs} \qquad (5)$$

where: I(Z,M) is the computed Kα X-ray yield per unit concentration per steradian per unit proton charge; the geometric part of the absolute efficiency and the proton charge calibration have been absorbed in the experimental constant H, leaving as explicit efficiency factors the intrinsic efficiency ε_Z^I and the attenuation in any absorbers.

This works well with specimens of known matrix composition. In micro-PIXE the standards must be homogeneous at the micron level, which is far from trivial to ensure. The agreement of H(Se) = 0.0285±0.0045 and H(Pd) = 0.0270±0.0011 in Remond's present synthetic pyrrhotite standard is a useful guarantor of accuracy, but the desirability of having several trace elements of widely spaced atomic number in the single standard is obvious.

This approach is related to that of computing a yield curve as a function of trace Z in a given matrix using eq. (1) and then normalizing the entire curve up or down by analyzing known standards; Clayton et al. (10) do this in recognition of uncertainties in current integration and absolute geometry.

A caution is necessary regarding the apparently innocuous final term in eq. (5). The

high counting rate of matrix characteristic X-rays and the concomitant pulse pile-up in many TTPIXE situations demands that a suitably chosen absorber (typically Aℓ) be interposed before the detector. Typical thicknesses of Aℓ used with mineralogical specimens are 0.3-0.8 mm (24). Manufacturers' thicknesses have ±10% tolerance and the thickness can vary significantly over a foil of a few cm^2 area; also μ/ρ values are accurate to only a few percent. Hence with a 500 μm Aℓ foil there is the possibility for example of incurring a 27% error in the Se Kα transmission.

Care is thus needed in characterizing the absorber. An average thickness found by simply weighing would not be appropriate given the thickness variations. A comparison of the I(Kβ)/I(Kα) with and without absorber for a target in the $20 < Z < 40$ region is one possibility that has the advantage of being done under the same conditions and using the same portion of the absorber as the actual TTPIXE analysis. Another possibility is to compare major element intensities in an alloy target with and without the absorber present.

A final calibration variant is to use a major matrix element of known concentration (via EPMA or stoichiometry) as internal standard for the TTPIXE analysis. When feasible this has the attraction of convenience, but it is imperative that the standard element chosen be homogeneously distributed. If the element is of low Z, accurate absorber characterization is extremely important since attenuation of its X-rays will be strong.

Minimum Detection Limits (MDL's) in TTPIXE

Most published PIXE work involves thin targets of light matrix, the background then consisting mainly of bremsstrahlung. In the thick target context one finds a greater preponderance of work with matrices of sufficiently high atomic number that the matrix characteristic X-rays play a major role in determining MDL's. The situation is complex and involves an interplay among various parameters including matrix Z, thickness of absorber used to attenuate matrix X-rays, counting rate, pulse pile-up, etc. It is, in general, not possible to optimize the MDL's simultaneously for elements of lower Z than the matrix and elements of higher Z than the matrix. A preliminary report on a comprehensive study of TTPIXE MDL's was recently presented (23). Here we simply discuss two figures (4,5) which convey a flavour of the results. These are for 2 MeV protons incident on Aℓ and Ge matrices. An on-demand beam deflector was used to minimize pulse pile-up. The detector solid angle was 0.013 sr and its resolution 172 eV at 5.9 keV.

In the Aℓ case, the beryllium windows of our chamber and detector were not quite sufficient to eliminate the intense Aℓ K X-rays, and results were taken with 25 and 120 μm aluminium absorbers. Clearly any absorber thickness beyond that required to suppress low-energy bremsstrahlung plus the Aℓ X-rays and

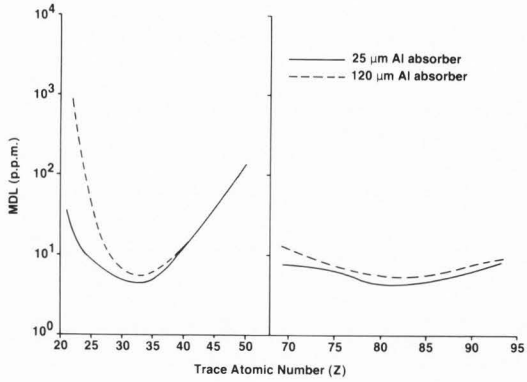

Fig. 4. Measured minimum detection limits using 2 MeV protons in an aluminum matrix as a function of trace element atomic number. The collected charge is 1 μC, corresponding to measurement times of 30 s with a 25 μm Aℓ absorber and 35 s with a 120 μm Aℓ absorber.

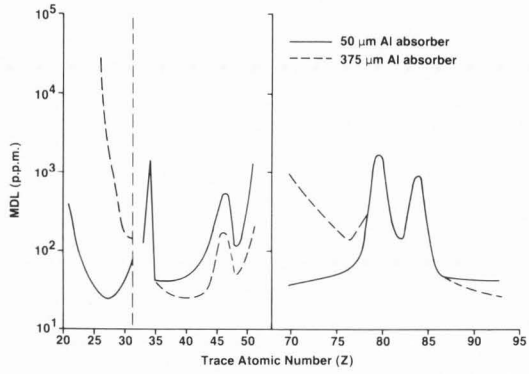

Fig. 5. Measured minimum detection limits using 2 MeV protons in a germanium matrix as a function of trace element atomic number. The collected charge is 1 μC, corresponding to measurement times of 45 m with a 50 μm Aℓ absorber and 6 m with a 375 μm Aℓ absorber.

their pile-up peaks, confers no advantage. For 1 μC of collected charge the best MDL is ~5 ppm in the $30 < Z < 35$ range and around $Z = 80$. The analysis times were only about half a minute (for 1 μC). A 30 m analysis would improve these MDL figures by a factor 7.7, providing sub-ppm limits in the optimum region of atomic number.

Fig. 5, for a Ge matrix, represents the situation where matrix X-rays are in roughly the middle of the spectrum. A rather thick absorber (375 μm) improves the MDL's of elements with $Z > 32$ by decreasing Ge K X-ray pile-up, but has little effect on the actual pile-up peaks. However this absorber provides very poor MDL's for $Z < 32$, where it is preferable to use the thinnest absorber that will keep bremsstrahlung

to a tolerable level. The MDL of course has maxima for elements whose K or L X-rays coincide in energy with Ge Kα or Kβ, and for obvious reasons no datum exists at Z = 32. For 1 μC charge, optimum levels of 25 ppm are reached in various atomic number ranges. Naturally the beam current can be greatly increased when the thicker absorber is used, resulting in our case in a decrease in analysis time from 45 to 6 minutes. Had one maintained 45 m analysis times, the MDL's with the thicker absorber would be $\sqrt{45/6}$ = 2.74 times lower.

The use of critical absorbers can provide further improvements for high-Z matrices at the cost of introducing extraneous X-rays into the spectrum. This is very relevant to analysis of archaeological alloys.

MDL comparisons between EPMA and PIXE are often naive and certainly dangerous. Many of PIXE's MDL's using energy-dispersive spectroscopy cannot be achieved by EPMA using energy dispersion; however substitution of wavelength dispersion in EPMA sometimes makes it competitive for trace elements; but then the same substitution in PIXE would restore the prior situation. We prefer to avoid this sort of argument and examine practical analytical situations. Remond et al. (24) do so in this volume for sulfide minerals using PIXE (energy dispersive) and EPMA (wavelength-dispersive). PIXE's advantage in this very specific context ranges from only ×2 up to ×30 depending on the element/matrix combination.

Unfolding of PIXE Spectra

Least-squares codes for fitting PIXE spectra and providing accurate Kα and Lα peak intensities are not yet in as widespread use as analogous EPMA codes. Those in use model the characteristic peaks by Gaussians, sometimes with tailing corrections, taking relative intensities for each element from theory (27), individual measurement or review (26). In the thick-target case these intensities must be adjusted for attenuation using eq. (1). This is straightforward if the matrix is known; if it is not known, an iterative approach is needed where the matrix concentrations are guessed, the fit done and concentrations deduced from peak intensities, and the cycle then repeated to consistency. Most codes also use analytical models for the bremsstrahlung background, but these are semi-empirical. There has not yet been an intensive effort to provide a universal formulation analogous to the various modifications of Kramer's Law used in EPMA. In at least one code (8) the widely used EPMA technique of removing background by a top-hat filter has been used for TTPIXE in preference to modelling the background: an advantage of this is the decrease in the number of parameters that must be varied during the fitting procedure.

The level of development reached is illustrated in a recent inter-comparison exercise (8) wherein five groups deployed very different fitting codes on a defined set of spectra measured on a well-characterised PIXE system. Most of these were from thin targets of low-Z matrix, which are not the target types under discussion here, but nonetheless ref. (8) provides a useful overview. The various codes incorporated varying data bases, peak models, background treatment and fitting methodologies. We shall not quote any numerical results, since improvements to at least two of the codes used render such numbers obsolete; instead we summarise the observed trends.

The fits to single-element standard spectra gave Kα peak intensities that agreed well for $20 < Z < 40$. At lower and higher Z observed differences indicated the need for better analytic description of peak tailing due to imperfect charge collection and to Compton scattering, respectively. The fitted peak intensities in multi-element spectra from various biological and environmental specimens were the main target of enquiry. For each element (typically 15) in each spectrum (12 in all) any given code's Kα peak intensity P was expressed relative to the mean $\bar{P}$ over the five codes. When each code's $P/\bar{P}$ were then averaged over all elements and all specimens, the resulting five figures of merit were typically only 1 or 2% different from unity. This is a remarkable and encouraging outcome, which should lend the user confidence in any PIXE fitting code that adopts a subset of the methods of ref. (8). There were, of course, occasional much larger differences (±15%) in peak areas, usually for weak peaks riding on the low-energy tails of intense neighbours, e.g., Mn Kα on Fe Kα. This observation indicates the need for improved analytic description of peak tailing arising both from charge collection imperfections and from radiative Auger satellites.

Currently we are using monochromatized photons in the 2 to 20 keV energy region to investigate the lineshape of Si(Li) detectors. The function:

$$F(i) = G(i) + D^{L}(i) + D^{S}(i) + E(i) \qquad (6)$$

where

$$G(i) = H_G \exp\left[-\frac{(i - i_o)^2}{2\sigma^2}\right] \qquad (7)$$

$$D^{L,S}(i) = \frac{1}{2} H_D^{L,S} \exp\left[\frac{i - i_o}{\beta_{L,S}}\right] \operatorname{erfc}\left[\frac{i - i_o}{\sigma\sqrt{2}} + \frac{\sigma}{\beta_{L,S}\sqrt{2}}\right] \qquad (8)$$

E(i) is the silicon escape peak, and i = channel number. We find excellent fits in the 4-20 keV energy region as exemplified by figure 6 for the spectrum of iron $K\alpha_1$, which contains 5×10^6 counts. Evidently the two exponential terms describe the low-energy tailing very well indeed; their height (H_D) and slope β parameters are smooth functions of energy, easing their incorporation into a PIXE spectrum fitting code. At lower energies figure 7 shows that eq. (6) is less successful; empirical addition of a broad Gaussian near 2 keV improves the Ag $L\alpha_1$ fit (2.98 keV energy), but extensive work is needed

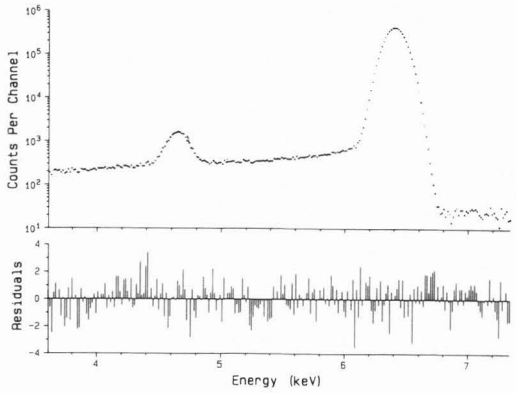

Fig. 6. Results of fit of eq. (7) to the iron $K\alpha_1$ line. Residuals are weighted by the square root of the error of the counts per channel.

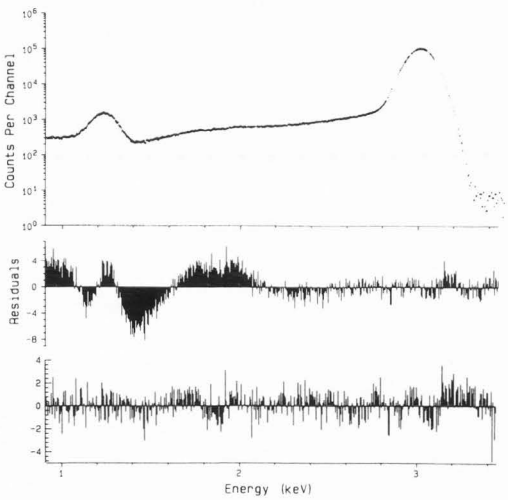

Fig. 7. Results of fit of eq. (7) to the silver $L\alpha_1$ line. Residuals are weighted by the square root of the error of the counts per channel. See text for detail of necessary modification of eq. (6) for the lower residual set.

to understand and parametrize lineshapes in the 1-4 keV region.

Analyses

Protons of 2.0 MeV were used to analyse the NBS aluminum alloy standard SRM 1258 and a specimen of gallium antimonide. Calibration was effected relative to thick, pure single-element standards, using eq. (4). For elements where no standard was available, Y_{ST} was obtained by interpolation on the measured curve of Y_{ST} as a function of Z. The aluminum was run at a 700 cps counting rate for 54 m with current 5.7 nA; the absorber was a 50 μm Aℓ foil. The GaSb was run at 1500 s^{-1} for 9.7 m using 9.5 nA current; the absorber here was 375 μm. Peak areas were obtained from the spectra by fitting with the Guelph PIXE software described in ref. (8).

The aluminum specimen tests TTPIXE's ability to deal with several trace elements, whose K X-ray peaks overlap (figure 8) in a known matrix. The GaSb is treated as a completely unknown matrix, necessitating an iterative solution of eq. (4).

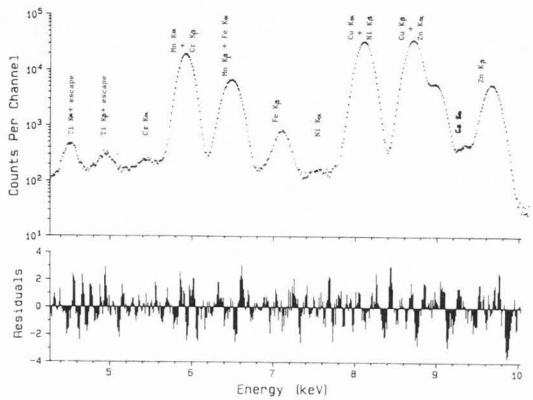

Fig. 8. PIXE spectrum of NBS aluminum alloy standard taken with 2.0 MeV protons.

Table 2 compares the TTPIXE results for the SRM together with the concentrations recommended by NBS and the MDL's from our earlier work scaled up to 18.5 μC charge. Given the quoted

Table 2

Concentration in % by weight for SRM 1258

Element	MDL	Concentration % by weight: Certified value	PIXE
Ti	0.005	0.04*	0.0384 (± 9%)+
Cr	0.0014	0.0011 (±19%)	0.0025 (±42%)
Mn	0.001	0.48 (± 2%)	0.4912 (± 2%)
Fe	0.0080	0.079 (± 4%)	0.0918 (± 4%)
Ni	0.0006	0.0006 (±50%)	0.0009 (±70%)
Cu	0.0006	0.84 (±1.2%)	0.8947 (± 2%)
Zn	0.0005	1.03 (± 1%)	1.1348 (± 2%)
Ga	0.0005	0.010*	0.0125 (±18%)

* Not sufficiently homogeneous for certification.

\+ Errors are 1σ equivalent

uncertainties (one standard deviation) the agreement between measured values and NBS data is reasonably good for Ti, Mn, Fe, Cu, Zn. The poorer agreement for Cr and Ni reflects the proximity of their concentrations to the MDL.

The weight fractions determined for GaSb are 0.352±0.01 and 0.648±0.01 for Ga and Sb, respectively. These agree well with the stoichiometric values of 0.364 and 0.636.

While there is room for improvement, both sets of results are encouraging.

Other Remarks

There have been two broad areas of activity in TTPIXE recently. One has been the deployment of the technique in major application areas such as mineralogy, geochemistry and archaeology. The other is the general development of methodology covered in this paper. In addition to these there are various interesting off-shoots worth mention.

Dahlmann et al. (14), motivated by the need to analyze archaeometric alloys (coins, jewellery) with curved surface structure, investigated the flat surface requirement of eq. (1) both experimentally and by computer simulation. They showed that the fundamental method provided correct results if two conditions were fulfilled. The inclination of the tangent plane of the curved surface at the beam impact point must be known; it can be determined by reflection of a laser beam. Secondly, the radius of curvature of the surface in the analysis area must be 3-4 times greater than the proton beam radius.

A related situation is that where a randomly rough specimen surface may not be interfered with, thus again violating the flat surface requirement of eq. (1). The ratio of characteristic trace element X-ray yields Y_r and Y_s from randomly rough and from smooth surfaces of given matrices has been obtained by computer simulation (7), typical results of which are shown in figure 9. The main determinant of the roughness-induced decrease in yield is expected to be the ratio σ/μ^{-1} where σ is the standard deviation in surface height about the mean and μ^{-1} the X-ray attenuation length. Hence Y_r/Y_s should be similar for matrix/emitter combinations that provide the same values of $\sigma\mu$, i.e., of $\sigma\rho(\mu/\rho)$. Figure 10 plots Y_r/Y_s versus μ/ρ for various matrices of a given $\sigma\rho$ value (equivalent to an Fe matrix with σ = 5 μm). The expectation of similar behaviour for these matrices as a function of μ/ρ is confirmed. For any matrix 'm' the roughness effect may be obtained as follows. The σ_m value corresponding to σ = 5 μm for iron is obtained as σ_m = $39.37/\rho_m$, and then the roughness results for this σ_m are essentially those of figure 9 for iron. Those for any other value of σ_m can be obtained from the observed scaling of loss of yield as $\sigma^{1.43}$.

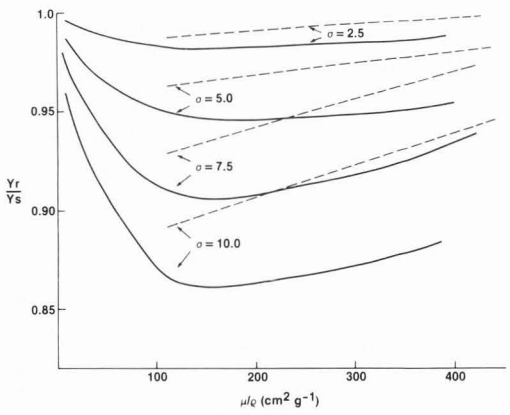

Fig. 9. Ratio of rough and smooth surface X-ray yields as a function of trace X-ray attenuation coefficient for 3 MeV protons incident on an iron matrix. θ_{TO} is 45°; σ represents standard deviation of surface height. Dashed curves are for trace elements lighter than iron and full curves for heavier trace elements.

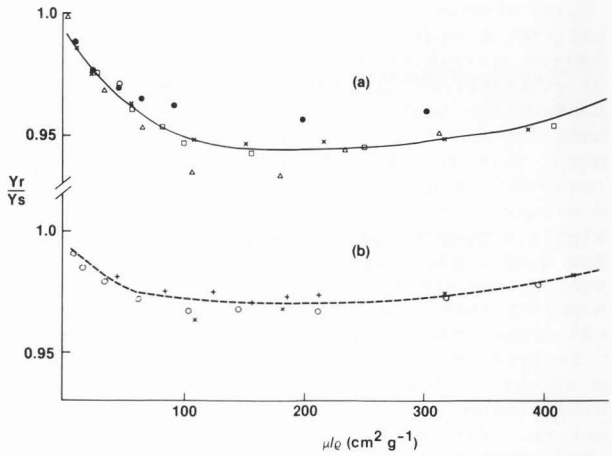

Fig. 10. Attenuation coefficient dependence of Y_r/Y_s for 3 MeV protons incident on a set of matrices having a common value of $\sigma\rho$. In addition to the 4 elements C (·), Fe (X), Ag (o), Pb (+), there are two compound matrices viz quartz (Δ) and hydroxy-apatite (□) or bone tissue. Curve (a) is for trace elements whose X-rays lie above the matrix K absorption edge and curve (b) for those falling below the edge.

A third interesting area is the development of secondary fluorescence corrections. Although rather routine in EPMA these are not yet so in TTPIXE. The first work was that of Reuter et al. (25), who by restricting calculations to normal proton incidence were able to give a straightforward expression whose numerical integration necessitated a significant computational overhead. For this reason they also provided an approximate version analogous to that used frequently in EPMA which could be quickly calculated. Re-examination of these with a modern data base would be useful. The small amount of work since then is reviewed in

ref. (4) and by Smit et al. (28). The latter authors present an analytical expression for secondary X-ray yields which they can incorporate into an overall analytic treatment for deriving concentrations from thick-target X-ray yields. Calculations with this model gave results in agreement with the more complex treatments in the earlier literature, and were supported by experiment.

Conclusions

This brief overview reveals the rapid approach to maturity of TTPIXE as an analytical technique. Despite the need for further work on peak modelling, on spectrum background and on tests via standard reference materials, TTPIXE can be used with confidence in growing application areas such as mineralogy and archaeometry.

References

(1) Andersen HH, Ziegler JF (1977) The stopping power and ranges of ions in matter, Vol. 3. Ziegler JF, (ed), Pergamon Press, New York.

(2) Bambynek W (1984) New evaluation of K-shell fluorescence yields. Proc. - X84 Int. Conf. on X-ray and inner-shell processes ion atoms, molecules and solids. Univ. of Leipzig.

(3) Brandt W, Lapicki G (1981) Energy-loss effect in inner-shell Coulomb ionization by heavy charged particles. Phys. Rev. A23, 1717-1727.

(4) Campbell JL, Cookson JA (1984) PIXE analysis of thick targets. Nucl. Instrum. Meth. B31,87-197.

(5) Campbell JL, McGhee PL (1986) State-of-the-art efficiency determination for a Si(Li) X-ray detector in the 3-40 keV energy range. Nucl. Instrum. Meth. A248, 393-404.

(6) Campbell JL, Cookson JA, Paul H (1983) Uncertainties in thick-target PIXE analysis. Nucl. Instrum. Meth. 212, 427-439.

(7) Campbell JL, Lamb RD, Leigh RG, Nickel BG, Cookson JA (1985) Effects of random surface roughness in PIXE analysis of thick targets. Nucl. Instrum. Meth. B12, 402-412.

(8) Campbell JL, Maenhaut W, Bombelka E, Clayton E, Malmqvist K, Maxwell JA, Pallon J, Vandenhaute J (1986) An inter-comparison of spectral data processing techniques in PIXE. Nucl. Instrum. Meth. B14, 204-220.

(9) Chen MH, Crasemann B (1985) Relativistic cross-sections for atomic K- and L-shell ionization by protons, calculated from a Dirac-Hartree-Slater model. At. Data Nucl. Data Tables 33, 217-233.

(10) Clayton E, Cohen DD, Duerden P (1981) Thick-target PIXE analysis and yield curve calculations. Nucl. Instrum. Meth. 180, 541-548.

(11) Cohen DD (1987) Average L shell fluorescence yields. Nucl. Instrum. Meth. B. In press.

(12) Cohen DD, Harrigan M (1986) Calculated L-shell X-ray line intensities for proton and helium ion impact. At. Data Nucl. Data Tables 34, 393-414.

(13) Cohen DD, Harrigan M (1985) K- and L-shell ionization cross-sections for protons and helium ions calculated in the ECPSSR theory. At. Data Nucl. Data Tables 33, 255-343.

(14) Dahlmann H, Fazly Q, Mommsen H, Weber A (1984) Particle induced X-ray emission analyses on metal samples with structured surfaces. Nucl. Instrum. Meth. B1, 41-44.

(15) Gerward L (1984) Empirical absorption formulae for use in X-ray spectrometric analysis: LTF III Report 49 (Tech. Univ. of Denmark, Lyngby).

(16) Hansteen JM, Kocbach L, Grave A (1985) Total K-shell Coulomb ionization cross-sections at very low projectile energies. Phys. Scripta 31, 63-68.

(17) Johansson SAE, Johansson TB (1976) Analytical application of particle-induced X-ray emission. Nucl. Instrum. Meth. 137, 473-516.

(18) Khan R, Karimi MM (1980) Kβ/Kα ratios in energy-dispersive X-ray emission analysis. X-Ray Spectrom. 9, 32-35.

(19) Krause MO (1979) Atomic radiative and radiationless yields for K and L shells. J. Phys. Chem. Ref. Data 8, 307-327.

(20) Leroux J, Thinh TP (1977) Revised tables of X-ray mass attenuation coefficients. Corp. Scientifique Claisse Inc, Québec.

(21) Paul H (1986) Tests of various theories for K-shell ionization by protons. Z. Phys. D4, 249-252.

(22) Paul H, Muhr J (1986) Review of experimental cross-sections for K-shell ionization by light ions. Phys. Reports 135, 47-97.

(23) Perujo A, Campbell JL, Maxwell JA (1987) A comprehensive study of detection limits in thick-target PIXE. Proc. 11th Int. Congress on X-ray optics and microanalysis, (eds), Brown JD, Packwood RH (Univ. of Western Ontario Graphics Services, London, Ontario) 151-155.

(24) Remond G, Cesbron F, Traxel K, Campbell JL, Cabri LJ (1987) X-ray spectrometry by means of EPMA and micro-PIXE applied to trace element analysis in sulfides: problems and prospects. Scanning Microsc., 1 (3), 1015-1035.

(25) Reuter W, Lurio A, Cardone F, Ziegler JF (1975) Quantitative analysis of complex targets by proton-induced X-rays. J. Appl. Phys. 46, 3194-3202.

(26) Salem SI, Panossian SL, Krause RA (1974) Experimental K and L relative X-ray emission rates. At. Data Nucl. Data Tables 14, 91-109.

(27) Scofield JH (1974) Exchange corrections of K X-ray emission rates. Phys. Rev. A9, 1041-1049.

(28) Smit Z, Budnar M, Cindro V, Ravnikar M, Ramsak V (1985) Secondary fluorescence corrections in thick target PIXE analysis. Nucl. Instrum. Meth. 228, 482-489.

Discussion with Reviewers

Reviewer I: What are the most pressing atomic physics questions to answer to improve the data

base for thick target PIXE?
Authors: The answer depends on one's preferences among standardization methods and on the specimen types used. If photon attenuation is the main source of uncertainty, then the emphasis would be on better μ/ρ interpolation schemes; one problem of such schemes in EPMA is that they often cover a more limited energy range than that needed for PIXE. The present exercise by the International Union of Crystallography, which is measuring μ/ρ for well-characterized specimens in various labs, will be of value for PIXE.

Our other personal preference would simply be for continued progress in refining L subshell ionization cross-sections, fluorescence yields etc. since L-shell data are certainly much less well known than the corresponding K-shell data.

Reviewer I: Should Rutherford backscattering measurements be incorporated in the experiment to get information on the sample matrix and sample surface roughness?
Authors: Yes, RBS measurements are of great value in characterizing light matrices and are a valuable complement to PIXE especially for low-Z elements. Thanks to the work of R.D. Edge and U. Bill, (1980) Nucl. Instrum. Meth. 168, 157 they can also give a measure of roughness in simple specimens. We are contemplating some experiments on roughness diagnosis combining both techniques.

Reviewer II: Attempts have been made to estimate depth profiles using TTPIXE. Could the authors please comment on the possibilities and limitations of such a technique.
Authors: In contrast to RBS, which is very powerful as regards depth profiling, PIXE has seen only limited use and in a semi-quantitative sense at that. One can vary the proton energy to sample varying depths, and a related approach is to use various beam impact angles α (see fig. 1). We recall that variation of the K_β/K_α intensity ratio due to matrix attenuation has also been used to estimate depth of X-ray production. These methods offer some potential if the trace element is localised as a thin layer at well-defined depth. But if it is distributed in some depth-dependent manner, none of the methods offers great potential. The problem in all these approaches is that the X-ray production is spread along the early portion of the proton track and hence this distribution is convoluted with the depth-profile.